Investigation of factors affecting isolation of needle-shaped particles in a vacuum agitated filter drier through non-invasive measurements by Raman spectrometry

Peter Hamilton,[a] David Littlejohn,[a]* Alison Nordon,[a]* Jan Sefcik,[b] Paul Slavin,[c] John Andrews[d] and Paul Dallin[d]

[a] WestCHEM, Department of Pure and Applied Chemistry and CPACT, University of Strathclyde, Glasgow, G1 1XL, UK

[b] Department of Chemical and Process Engineering, University of Strathclyde, 75 Montrose Street, Glasgow, G1 1XJ, UK

[c] GlaxoSmithKline, Gunnels Wood Road, Stevenage, Hertfordshire, SG1 2NY, UK

[d] Clairet Scientific, 17/18 Scirocco Close, Moulton Park Industrial Estate, Northampton, NN3 6AP, UK

* denotes authors to whom correspondence should be sent

David Littlejohn

Email: d.littlejohn@strath.ac.uk; tel: +44(0)141 548 2067; fax: +44(0)141 548 4212

Alison Nordon

Email: alison.nordon@strath.ac.uk; tel: +44(0)141 548 3044; fax: +44(0)141 548 4212

Abstract

The effects of pressure filtration and vacuum agitated drying on cellobiose octaacetate (COA) particles in methanol slurries were studied by making Raman measurements through the glass wall at the side of a filter drier beneath the oil jacket. The change in intensity of methanol peaks in the spectra allowed the removal of the solvent from the particle bed to be monitored. Also, drying curves for COA generated from the Raman measurements gave an indication of the changing physical status of the particle bed during continuous or intermittent agitation. The intensity of the Raman signal for COA depended on the bulk density of the particle bed, which changed due to aggregation and attrition that occurred during solvent removal and particle motion induced by agitation during vacuum drying. Loss on drying (LOD) measurements of samples removed at the end of the pressure filtration and vacuum agitated drying stages established the degree of wetness and confirmed the end point of drying (<0.5% w/w solvent), respectively. Dynamic image analysis confirmed that minimum attrition of COA was achieved when (a) the majority of the methanol was removed during pressure filtration at 0.5 bar N_2 and (b) intermittent agitation was applied during the vacuum drying stage.

Keywords

Raman spectrometry; process analytical technologies (PAT); filtration; drying; particle processing; attrition.

1. Introduction

The use of agitated filter driers is popular for isolation of active pharmaceutical ingredients (APIs) following crystallisation, as filtration and drying can be completed in a single vessel (Kougoulos et al., 2011). Industrial filtration is often performed under a positive pressure of an inert gas, typically N_2, to remove excess solvent from particles before drying is conducted under vacuum to remove the remaining residual solvent. The impact of the isolation process on particulate properties, especially during the drying phase, may determine the success of an API manufacturing campaign; however, the effects of particle isolation are often not well understood and poorly controlled.

There are a growing number of examples in the literature where the influence of agitated drying on particulate properties has been investigated (Hare et al., 2009; Kom et al., 2011; Kougoulos et al., 2011; Lamberto et al., 2011; Lekhal et al., 2003; Lekhal et al., 2004). The processes that lead to particle attrition have been studied extensively by Ghadiri et al. (Ghadiri et al., 2000; Ghadiri et al., 1991; Ghadiri and Zhang, 2002; Subero and Ghadiri, 2001; Zhang and Ghadiri, 2002). Lamberto et al. (2011) reported the development of a laboratory method to rank qualitatively six pharmaceutical materials on a breakage scale (hard, medium or easy to break) that allowed recommendations for processing conditions at a larger scale. In contrast, there have been few published studies of the combined effects of filtration and agitated drying on particulate properties. Recently, however, needle breakage has been reported at the end of filtration of needle-shaped particles, owing to the stress caused by the positive pressure applied to the particles exceeding that of the critical stress required for needle breakage (MacLeod and Muller, 2012).

Process analytical technologies (PAT) are currently being implemented across a wide range of unit operations in the pharmaceutical industry to improve process understanding and

control. Various spectroscopic techniques have been applied successfully to monitor unit operations such as crystallisation (Cornel et al., 2008; Kougoulos et al., 2005; Larsen et al., 2006; Liu et al., 2011; O'Grady et al., 2008), granulation (De Beer et al., 2011; Tok et al., 2008; Walker et al., 2009) and blending (El-Hagrasy et al., 2006a; El-Hagrasy et al., 2006b; El-Hagrasy and Drennen, 2006). Drying processes have also been studied either through analysis of the off-gas or the particle bed directly. For example, optical spectroscopic techniques such as mid infrared (MIR) (Tewari et al., 2010) and near infrared (NIR) (Coffey et al., 1998; Harris and Walker, 2000; Parris et al., 2005) have been used to monitor the solvent concentration in the off-gas of tray and rotary driers by insertion of a gas cell into the vacuum line. On-line mass spectrometry has also been used to measure the moisture content in the off-gas for microwave assisted vacuum drying (Hettenbach et al., 2004). The solvent content of the particle bed in filter, paddle and spherical driers has been monitored *in situ* using an in-line NIR probe (Burgbacher and Wiss, 2008). In-line NIR spectrometry has also been used to monitor the progress of fluidised bed drying processes (Demers et al., 2012; Green et al., 2005; Peinado et al., 2011). In all of the above studies, the extent of drying was monitored on the basis of the solvent content of either the off-gas or powder bed. However, in one study the drying of molecular sieves in a rotary drier was monitored using acoustic emission generated from the impact of the particles with the vessel wall (Briens et al., 2008). The effects of the drying conditions on the particles themselves are rarely considered and the physical effects that occur during drying are still relatively unstudied. Spectra obtained with near-infrared (NIR) or Raman spectroscopy are known to be affected by the physical properties of samples and have been used in powder blending (Bellamy et al., 2008a; Bellamy et al., 2008b) or wet granulation (Walker et al., 2009) to study physical changes to the material. Raman spectrometry can offer advantages over NIR spectrometry including narrower spectral features and easier interpretability of the spectra (Allan et al., 2013). For

isolation processes, Raman spectrometry provides opportunities to monitor directly and simultaneously both the solvent and powder. Drying end-point is currently determined by off-line measurement of the solvent content of the powder bed, which is sampled periodically during the process. Consequently, *in situ* measurements eliminate the need for sampling and also allow identification of the drying end-point in real-time; the ability to monitor both solvent removal and the physical state of the powder bed allows better control of particle properties. Benefits of implementation of PAT for drying processes include a reduction in drying time, elimination of over-drying, and lower energy consumption and costs (Parris et al., 2005).

In a preliminary study (Hamilton et al., 2011), methods were investigated for monitoring needle-shaped cellobiose octaacetate (COA) particles directly in a laboratory scale vacuum agitated drier using non-invasive Raman spectrometry. A design of experiments approach was used to investigate the effects of three process variables (mode of agitation, % solvent loss on drying, and jacket temperature) on the drying time, with off-line particle size analysis by laser diffraction employed to determine the extent of attrition. Subsequent research compared the efficacy of three commonly used particle size analysis techniques for quantitative assessment of the extent of attrition that occurs during the drying of needle-shaped particles (Hamilton et al., 2012). It was found that the Feret Max diameter obtained from dynamic image analysis provided the best indication of changes in needle length; although qualitative trends could be obtained from laser diffraction or focused beam reflectance measurements.

In this study, the full isolation process for filtration and drying of COA particles in a vacuum agitated drier was investigated. Slurries of COA particles and methanol were subjected to different periods of pressure filtration before vacuum agitated drying was performed using either continuous or intermittent agitation. Raman measurements were collected *in situ*

116 throughout each experiment and samples were collected at the end of each stage for
117 measurement of loss on drying (LOD) and particle size using dynamic imaging analysis. In
118 contrast to the preliminary study (Hamilton et al., 2011), Raman measurements were made
119 from the side of the vessel towards the bottom of the packed bed rather than from the top,
120 which allowed a better assessment of the impact of the filtration/drying conditions on the
121 particles during processing. By interpretation of the Raman profiles it was possible to monitor
122 in real time the removal of the solvent and changes to the physical status of the packed bed,
123 and hence determine the end point of drying. Further, the particle size analysis allowed the
124 relationship between starting wetness (LOD), agitation time and extent of attrition to be
125 examined. The study illustrates for the first time the potential of non-invasive Raman
126 spectrometry to monitor the full filtration-drying isolation process, which will be particularly
127 beneficial when optimising conditions for fragile particles.

128

2. Materials and methods

2.1. Materials

Cellobiose octaacetate (COA) was obtained from GSK (Stevenage, Hertfordshire, UK). COA has a needle-shaped crystal habit with a high aspect ratio and does not exhibit polymorphism. COA was selected as a model compound to study as it has similar physical characteristics to many pharmaceutical active compounds (e.g. the dry powder has a low bulk and tapped density and the crystals are needle-shaped), without being biologically active and therefore requires no specific controls for handling in a laboratory. Methanol (Sigma-Aldrich, A5376, Dorset, UK) was chosen as the liquid phase for this study as it is often used as an anti-solvent in the re-crystallisation of COA. A cylinder of oxygen-free nitrogen gas (BOC) was used for pressure filtration.

2.2. Lab scale filter drier

A schematic of the drier is shown in Fig.1. The drier is made of glass, has an internal diameter of 15 cm and is based on process scale agitated filter driers (Hamilton et al., 2011). The agitator has two angled retreat blades (polytetrafluoroethylene (PTFE)) positioned at 180°. The motor is an IKA RW 20 digital (IKA works, Wilmington, USA), which was positioned at 90° to the vessel and drove the agitator through a 10 : 1 gear box at a mixing speed of 10 rpm. Oil heated to 60 °C by a Haake DC5/ K20 heater/chiller unit (ThermoHaake, UK) was pumped through the jacket of the reactor. For the experiments described in this work, 250 g of COA was transferred to a 2 L conical flask before 1 L of methanol was added. The resulting slurry was transferred from the conical flask into the drier through a port in the lid; the conical flask was rinsed with 100 mL of methanol, which was then transferred into the vessel before the port was sealed. A positive pressure of N_2 at 0.5 bar was applied to the slurry for 0, 0.167 (10 min), 0.333 (20 min), 0.5 (30 min) or 1 h and

153 methanol was collected in a solvent reservoir in the line. In the initial experiment (0 h), the
154 cake was allowed to filter for 1 h at atmospheric pressure prior to moving to the vacuum
155 agitated drying stage. At the end of the pressure filtration step for each experiment, a sample
156 was extracted for LOD and particle size analysis; the base of the drier was then connected to
157 a vacuum pump and the line was switched, using a PTFE T-junction with two taps, to collect
158 in a cold finger the remaining solvent that was not removed during pressure filtration. The
159 vacuum was held between 50 – 100 mbar during vacuum drying; the pressure was monitored
160 using a Pirani gauge (Edwards, Crawley, UK) in the line. During vacuum drying, continuous
161 or intermittent (1 min every 0.5 h) agitation of the particles was carried at a mixing speed of
162 10 rpm. Interpretation of the Raman spectra collected throughout the isolation process
163 indicated when the powder was dry. At this point, a second sample was extracted for LOD
164 and particle size analysis.

165 **2.3. Loss on drying analysis**

166 A sample thief probe was made by cutting the bulb of a plastic pipette tip; to obtain a sample,
167 the bulb was inserted and filled with powder from the vessel. The total weight of sample was
168 measured on collection and after static drying in an oven at ~100 °C (to give the weight of
169 solids in the sample). The LOD is the weight lost during drying expressed as a percentage of
170 the weight of solids in the sample. After oven drying and LOD analysis, the samples were
171 subjected to particle size analysis.

172 **2.4. Particle size analysis**

173 Sympatec QICPIC image analysis (Sympatec Ltd, Bury, UK) was performed on the COA
174 particles before the slurries were prepared, after each N_2 pressure filtration period, and after
175 each vacuum agitated drying period using the LIXELL wet dispersion unit. Powder was
176 dispersed in 0.1% Tween 80 (SigmaAldrich, UK) in water and circulated through a flow cell

177 using a peristaltic pump. A pulsed light source was used to ensure that no motion blur of the
178 particles occurred as they were imaged onto a CCD detector. WINDOX 5 software
179 (Sympatec Ltd) was used to perform the measurements (30 s) and analyse the data. The
180 particle size dimension used in this study was the Feret Max diameter (Hamilton et al., 2012)
181 and the results quoted are an average of three measurements from the same sub-sample.

182 **2.5. Non-invasive Raman spectrometry**

183 A Kaiser RXN1 Raman spectrometer with P^{h}AT probe (Kaiser Optical Systems Inc., Ann
184 Arbor, USA) was used to monitor the drying process non-invasively. The P^{h}AT probe has the
185 laser beam optically expanded to give a 6 mm spot size, a working distance of 25.4 cm and a
186 depth of field of 5 cm. The beam was directed at the process through the glass wall (thickness
187 of approximately 1.5 cm) beneath the oil jacket at the side of the vessel as shown in Fig. 1.
188 The laser wavelength was 785 nm produced by an Invictus diode laser operated at 400 mW at
189 the source (equating to ~220 mW at the sample). A 1024 × 256 pixel CCD detector cooled to
190 -40 °C by a Peltier cooling system was also used. The Raman signal is divided into 10
191 channels that are imaged on the different tracks of the CCD camera.

192 Daily diagnostic tests were performed (which measured relative peak intensity and peak
193 position against known peaks from a cyclohexane standard) using the external sample
194 compartment accessory for the instrument. Raman spectra were recorded using iC Raman
195 software (Metler-Toledo, Columbus, USA) and exported as individual .SPC files to
196 MATLAB version R2010b (Mathworks, Natick, USA) for analysis using PLS_Toolbox
197 version 4.11 (Eigenvector Research, Washington, USA). Each Raman spectrum was recorded
198 with a 30 s integration time resulting in one spectrum every 35 s. For all Raman experiments,
199 the vessel was wrapped in aluminium foil to prevent room light from affecting the spectra.

When 1st derivative transformations were performed, a Savitzky-Golay function with a smoothing filter width of 11 points and 2nd order polynomial fit was applied.

When continuous agitation was applied, the powder was deemed to be dry when the 1st derivative Raman signal from COA at 1076 cm^{-1} and the ratio of methanol: COA peaks (1036 cm^{-1} : 904 cm^{-1}) in the underivatised Raman spectra were both constant (as defined later in section 3.2) for 0.167 h. With intermittent agitation, the same measurements were used to indicate the end point of drying, however, in this case the requirement was for a constant value of the methanol : COA peak ratio and a negligible change (<10%) in the signal from COA (1076 cm^{-1}) during and after the 1 min agitation period.

3. Results and discussion

3.1. N_2 pressure filtration stage

The conditions used during the study are shown in Table 1. In the experiments, an initial N_2 pressure filtration period was followed by a period of vacuum agitated drying that was terminated when the powder was deemed to be dry based on the combination of Raman measurements outlined in section 2.5. The data from experiments 1 – 5 in Table 1 show that most of the solvent was removed after a pressure filtration period of 0.5 h. The filtration periods for experiments 2 and 6 were the same (0.167 h), but the LOD values were different; a similar observation applies to the results for experiments 4 and 7 (filtration period of 0.5 h). The poor repeatability of LOD probably occurred due to differences in the effective pressure of N_2 owing to a small leak in the drier during experiments 6 and 7. Variations in the extent of solvent removal during fixed periods of pressure filtration are not uncommon and so it can be difficult to predict the end-point particularly during process scale up. Therefore, the ability to determine the solvent content without removing material from the drier would be beneficial. Furthermore, as the solvent load at the start of vacuum agitation influences the time required to dry the powder, it would also be useful to be able to detect the end-point of drying in real time.

Non-invasive Raman measurements were made throughout each pressure filtration period. Underivatised and 1st derivative Raman of COA and methanol can be found in Fig. S1a and Fig. S1b, respectively, of the Supplementary Information. A full assignment of the main peaks in the underivatised spectra is also given. Shown in Fig. 2a and Fig. 2b are example underivatised and 1st derivative Raman spectra (550 – 1250 cm^{-1}), respectively, recorded during experiment 5 (1 h pressure filtration). A large background arising from the glass wall of the vessel was observed above approximately 1150 cm^{-1} in all Raman spectra as shown in

Fig. 2a. The signal at 733 and 738 cm^{-1} in Fig. 2a and Fig. 2b, respectively, can be attributed to the PTFE agitator. The associated univariate curves from the methanol peak centred at 1044 cm^{-1} and the COA peak centred at 1076 cm^{-1} in the 1st derivative spectra are given in Fig. 3. Drying curves obtained for COA using the peaks at 910 and 1750 cm^{-1} in the 1st derivative spectra were comparable to that shown in Fig. 3a. The increase in the COA signal in Fig. 3 is attributable to two processes that occurred as the methanol was removed under pressure, i.e. there was a decreasing amount of methanol to contribute to the Raman scattering and the bulk density of the COA particles increased as the static bed of particles became more densely packed. At the commencement of the pressure filtration period there was an excess of methanol in relation to COA particles in the slurry, hence the low starting intensity of the COA peak. When the positive pressure was applied, the solvent was removed rapidly which compressed the COA particles into a packed bed of wet particles, resulting in a substantial reduction in the signal for methanol and a sharp rise in the signal for COA. The densification process continued as more of the methanol was removed and the COA signal continued to increase, albeit more slowly. Similar relative changes in the two Raman signals were noted for the other periods of pressure filtration, but to different extents. At the end of each pressure filtration phase, a sample was extracted for LOD and particle size analysis. The LOD data for each experiment are given in Table 1 and the LOD values are plotted against the univariate Raman signal for methanol at 1044 cm^{-1} (from 1st derivative spectra) in Fig. 4. Fig. 4 shows that a correlation exists between the LOD values and the Raman signal for methanol at the end of the pressure filtration period. This demonstrates that the Raman signal can be used to estimate the amount of remaining solvent in the drier, and it follows that Raman measurements could then be used to control pressure filtration so that a specific target range of LOD could be achieved without performing LOD measurements at defined time points.

Examples of the particle size distribution data for two experiments (pressure filtration times of 0.167 (experiment 2) and 1 h (experiment 5)) are shown in Fig. 5 along with the size distribution of the initial particles before preparation of the slurry. Also, the median (D50) Feret Max diameter of the particles after pressure filtration is given in Table 2 for each experiment. The particle size distribution data obtained from dynamic image analysis indicated a small increase in the number of shorter needles and fewer larger needles after pressure filtration. However, the extent of needle breakage was not significant for the time periods investigated when the filtration pressure was 0.5 bar. For significant needle breakage to occur, the applied pressure would have had to exceed the critical stress required to create fractures or failure modes in the particles (MacLeod and Muller, 2012). From comparison with similar compounds, the maximum stress developed in the particles with a pressure of 0.5 bar is of the order of 1 – 4 MPa (MacLeod and Muller, 2012), which is lower than the tensile strength (typically 5 – 14 MPa) of many common pharmaceutical materials (Roberts et al., 1995).

3.2. Vacuum agitated drying period

Non-invasive Raman spectrometry successfully identified the end-point of powder drying using the procedures outlined in section 2.5. The LOD values of the powders at the end of each vacuum agitated drying period were ≤ 0.5% w/w (Table 1). In this study, the drying end point was decided by the operator observing the Raman signals on a monitor, however, if the procedure were to be implemented in a real process, algorithms (such as moving block standard deviation analysis (Sekulic et al., 1998)) could be established in statistical software to automatically identify the end of drying. After completion of the experiments, data were also analysed using principal component analysis (PCA). However, PCA did not offer any additional information to that obtained using univariate analysis and so will not be discussed further.

As well as indicating when the end point of drying had been reached, the profiles of the drying curves obtained from the Raman spectra also give information about the physical status of the particle bed during vacuum agitated drying. This is illustrated in Figs. 6 and 7 for continuous (experiment 2) and intermittent (experiment 6) agitation, respectively. In each figure, the signal for COA at 1076 cm^{-1} in the first derivative spectra is overlaid with a drying curve based on the ratio of the underivatised intensities of MeOH: COA at 1036 and 904 cm^{-1}, respectively. Drying curves showing the removal of methanol could also have been established by plotting the 1^{st} derivative Raman signal at 1044 cm^{-1} versus time. Both peak ratio and univariate drying curve methods have been reported previously (Hamilton et al., 2011). In this study, the peak ratio method was preferred because the effects of particle motion were normalised, and therefore, a smoother drying curve was produced which was easier to interpret. The Raman intensities of COA recorded during the pressure filtration step are included in Figs. 6 and 7 and reflect the influence that removal of most of the methanol had on the bulk density of the COA, as described in section 3.1.

At the start of vacuum drying, a reduction in COA Raman signal was observed at the onset of agitation, which was again attributable to bulk density effects. The motion of the agitator induced a shear force that disrupted the packed bed and decreased the number of particles in the Raman measurement volume. The sharp increase in the signal observed at about 0.22 h in Fig. 6 can be attributed to a dense volume of particles passing through the laser beam as the packed bed was broken up. During the period of continuous agitation from 0.25 to 0.45 h in Fig. 6, a combination of particle attrition and aggregation caused the bulk density of the material sampled by the Raman laser to increase, resulting in an increase in the Raman intensity of COA. The maximum COA signal (at 0.45 – 0.60 h in Fig. 6) occurred when the methanol concentration was at a critical point where there was a maximum in the formation of liquid bridges between particles. The data in Fig. 4 suggests that the methanol

309 concentration at the critical point was ~5% w/w. After the critical point, the aggregates began
310 to break up, which reduced the bulk density of the material and caused the COA signal to
311 decrease again until a constant value was reached near the drying end point (from about
312 1.25 h in Fig. 6).

313 The drying curve for intermittent agitation, shown in Fig. 7, has some features similar to the
314 trends for continuous agitation. After pressure filtration, the first 1 min period of intermittent
315 agitation disrupted the packed bed, which reduced the bulk density and the COA Raman
316 signal, similar to that observed in the initial period of continuous agitation. There was then a
317 static period where removal of the solvent under vacuum caused partial re-compression of the
318 bed and so there was an increase in the Raman signal for COA until a steady state was
319 reached. By the second 1 min period of agitation (at around 0.833 h in Fig. 7), aggregation
320 effects began to dominate causing a marked increase in the bulk density of the sampled
321 material and so the COA Raman signal increased. As there was little remaining solvent to
322 remove, there was not a significant change in the Raman signal during the second static
323 period, but when agitation resumed further aggregation occurred, increasing the Raman
324 signal. Eventually, the aggregated material began to break up during the 1 min agitation
325 periods and dry powder was produced (by about 2.83 h in Fig. 7).

326 As the intensity of the Raman signal for COA was affected by both aggregation and attrition,
327 it was not possible to monitor the extent of attrition using *in situ* Raman measurements.
328 Therefore, samples were extracted at the end of the vacuum agitated drying period of each
329 experiment for LOD and particle size analysis. Example particle size distributions based on
330 the Feret Max dimension from dynamic image analysis are given in Fig. 8 for the initial
331 particles before the slurries were prepared and for particles from experiments 2 and 6. The
332 D50 median Feret Max values of the particles removed at the end of the pressure filtration
333 step and the vacuum agitated drying stage are given in Table 2. As previously mentioned,

little particle attrition occurred during pressure filtration as indicated by the D50 values in Table 2. However, the particle size distributions and D50 values showed that considerable attrition occurred during vacuum drying with continuous agitation, whereas the extent of attrition was much less for intermittent agitation. This is due to the significant differences in the shear forces that the particles are exposed to during the different modes of agitation.

The experiments carried out during this study allowed further investigation of the relationship between particle attrition and the agitation time (Fig. 9a) and the solvent load (particle wetness) at the start of agitation (Fig. 9b). Fig. 9 combines the data from the continuous and intermittent agitation experiments. The results displayed in Fig. 9a show that particle attrition occurred within the first 0.5 h of agitation, but thereafter, additional periods of agitation did not cause significant further attrition. At the start of agitation there were a high number of long needles present in all of the samples, and these long needles were most susceptible to fragmentation caused by collisions with the agitator, the vessel wall or other particles. At this stage, the attrition rate was high due to the low density and high friability of the COA particles. The D50 values did not change much beyond 0.5 h of agitation because by then the majority of the longer needles had undergone the attrition process, and the increase in the bulk density of the particles through aggregation reduced the shear sensitivity of the particles. The relationship between particle attrition and starting LOD (i.e. particle wetness) was also investigated and is shown in Fig. 9b. There does not seem to be a significant difference between the extent of particle attrition and LOD for the continuously agitated experiments, with significant particle breakage occurring under all the conditions studied. However, for intermittent agitation the starting LOD has a greater influence on attrition as more 0.5 h periods of agitation are required to dry wetter particles, increasing the likelihood of particle breakage due to the shear forces induced by the agitator.

4. Conclusions

The non-invasive Raman measurements, made through the glass wall beneath the oil jacket, allowed changes in the bulk density caused by particle motion and particle wetness to be monitored, and so the progression of drying could be tracked in real-time better than in previous investigations (Hamilton et al., 2011). As variations in the extent of solvent removal during fixed periods of pressure filtration and drying are not uncommon, the ability to monitor directly solvent removal and the effects of process conditions on the particle bed allows better control of particle properties, particularly when the compound is susceptible to significant attrition and agglomeration effects.

Acknowledgements

The authors would like to thank GSK, Clairet Scientific and the University of Strathclyde EPSRC CTA scheme for funding for the project and Sympatec GMBH for allowing the samples to be analysed with QICPIC. AN thanks the Royal Society for the award of a University Research Fellowship.

374 **References**

375 Allan, P., Bellamy, L.J., Nordon, A., Littlejohn, D., Andrews, J., Dallin, P., 2013. In situ
376 monitoring of powder blending by non-invasive Raman spectrometry with wide area
377 illumination. Journal of Pharmaceutical and Biomedical Analysis 76, 28-35.

378 Bellamy, L.J., Nordon, A., Littlejohn, D., 2008a. Effects of particle size and cohesive
379 properties on mixing studied by non-contact NIR. International Journal of Pharmaceutics
380 361, 87-91.

381 Bellamy, L.J., Nordon, A., Littlejohn, D., 2008b. Real-time monitoring of powder mixing in a
382 convective blender using non-invasive reflectance NIR spectrometry. Analyst 133, 58-64.

383 Briens, L., Smith, R., Briens, C., 2008. Monitoring of a rotary dryer using acoustic emissions.
384 Powder Technology 181, 115-120.

385 Burgbacher, J., Wiss, J., 2008. Industrial applications of online monitoring of drying
386 processes of drug substances using NIR. Organic Process Research and Development 12,
387 235-242.

388 Coffey, C., Predoehl, A., Walker, D.S., 1998. Dryer effluent monitoring in a chemical pilot
389 plant via fiber-optic near-infrared spectroscopy. Applied Spectroscopy 52, 717-724.

390 Cornel, J., Lindenberg, C., Mazzotti, M., 2008. Quantitative application of in situ ATR-FTIR
391 and Raman spectroscopy in crystallization processes. Industrial and Engineering Chemistry
392 Research 47, 4870-4882.

393 De Beer, T., Burggraeve, A., Fonteyne, M., Saerens, L., Remon, J.P., Vervaet, C., 2011. Near
394 infrared and Raman spectroscopy for the in-process monitoring of pharmaceutical production
395 processes. International Journal of Pharmaceutics 417, 32-47.

396 Demers, A.M., Gosselin, R., Simard, J.S., Abatzoglou, N., 2012. In-line near infrared
397 spectroscopy monitoring of pharmaceutical powder moisture in a fluidised bed dryer: An
398 efficient methodology for chemometric model development. Canadian Journal of Chemical
399 Engineering 90, 299-303.

400 El-Hagrasy, A.S., D'Amico, F., Drennen, J.K., 2006a. A process analytical technology
401 approach to near-infrared process control of pharmaceutical powder blending. Part I: D-
402 optimal design for characterization of powder mixing and preliminary spectral data
403 evaluation. Journal of Pharmaceutical Sciences 95, 392-406.

404 El-Hagrasy, A.S., Delgado-Lopez, M., Drennen, J.K., 2006b. A process analytical technology
405 approach to near-infrared process control of pharmaceutical powder blending: Part II:
406 Qualitative near-infrared models for prediction of blend homogeneity. Journal of
407 Pharmaceutical Sciences 95, 407-421.

408 El-Hagrasy, A.S., Drennen, J.K., 2006. A process analytical technology approach to near-
409 infrared process control of pharmaceutical powder blending. Part III: Quantitative near-
410 infrared calibration for prediction of blend homogeneity and characterization of powder
411 mixing kinetics. Journal of Pharmaceutical Sciences 95, 422-434.

412 Ghadiri, M., Ning, Z., Kenter, S.J., Puik, E., 2000. Attrition of granular solids in a shear cell.
413 Chemical Engineering Science 55, 5445-5456.

414 Ghadiri, M., Yuregir, K.R., Pollock, H.M., Ross, J.D.J., Rolfe, N., 1991. Influence of
415 processing conditions on attrition of NaCl crystals. Powder Technology 65, 311-320.

416 Ghadiri, M., Zhang, Z., 2002. Impact attrition of particulate solids. Part 1: A theoretical
417 model of chipping. Chemical Engineering Science 57, 3659-3669.

418 Green, R.L., Thurau, G., Pixley, N.C., Mateos, A., Reed, R.A., Higgins, J.P., 2005. In-line
419 monitoring of moisture content in fluid bed dryers using near-IR spectroscopy with
420 consideration of sampling effects on method accuracy. Analytical Chemistry 77, 4515-4522.

421 Hamilton, P., Littlejohn, D., Nordon, A., Sefcik, J., Slavin, P., 2012. Validity of particle size
422 analysis techniques for measurement of attrition of needle-shaped particles that occurs during
423 vacuum agitated powder drying. Analyst 137, 118-125.

424 Hamilton, P., Littlejohn, D., Nordon, A., Sefcik, J., Slavin, P., Dallin, P., Andrews, J., 2011.
425 Studies of particle drying using non-invasive Raman spectrometry and particle size analysis.
426 Analyst 136, 2168-2174.

427 Hare, C.L., Ghadiri, M., Dennehy, R., Collier, A., 2009. Particle breakage in agitated dryers,
428 in: Nakagawa, M., Luding, S. (Eds.), Powders and grains. Amer Inst Physics, Melville, pp.
429 851-854.

430 Harris, S.C., Walker, D.S., 2000. Quantitative real-time monitoring of dryer effluent using
431 fiber optic near-infrared spectroscopy. Journal of Pharmaceutical Sciences 89, 1180-1186.

432 Hettenbach, K., Ende, D.J.A., Dias, E., Brenek, S.J., Laforte, C., Barnett, S.M., 2004.
433 Microwave assisted vacuum drying and endpoint determination using mass spectrometry,
434 part II, on-line moisture content profiling. Organic Process Research & Development 8, 867-
435 872.

436 Kom, P.K., Cook, W., Kougoulos, E., 2011. Impact of laboratory vacuum contact drying on
437 material drying rates and physical properties. Organic Process Research and Development 15,
438 360-366.

439 Kougoulos, E., Chadwick, C.E., Ticehurst, M.D., 2011. Impact of agitated drying on the
440 powder properties of an active pharmaceutical ingredient. Powder Technology 210, 308-314.

441 Kougoulos, E., Jones, A.G., Jennings, K.H., Wood-Kaczmar, M.W., 2005. Use of focused
442 beam reflectance measurement (FBRM) and process video imaging (PVI) in a modified
443 mixed suspension mixed product removal (MSMPR) cooling crystallizer. Journal of Crystal
444 Growth 273, 529-534.

445 Lamberto, D.J., Cohen, B., Marencic, J., Miranda, C., Petrova, R., Sierra, L., 2011.
446 Laboratory methods for assessing API sensitivity to mechanical stress during agitated drying.
447 Chemical Engineering Science 66, 3868-3875.

448 Larsen, P.A., Rawlings, J.B., Ferrier, N.J., 2006. An algorithm for analyzing noisy, in situ
449 images of high-aspect-ratio crystals to monitor particle size distribution. Chemical
450 Engineering Science 61, 5236-5248.

451 Lekhal, A., Girard, K.P., Brown, M.A., Kiang, S., Glasser, B.J., Khinast, J.G., 2003. Impact
452 of agitated drying on crystal morphology: KCl-water system. Powder Technology 132, 119-
453 130.

454 Lekhal, A., Girard, K.P., Brown, M.A., Kiang, S., Khinast, J.G., Glasser, B.J., 2004. The
455 effect of agitated drying on the morphology of L-threonine (needle-like) crystals.
456 International Journal of Pharmaceutics 270, 263-277.

457 Liu, X.S., Sun, D., Wang, F., Wu, Y.J., Chen, Y., Wang, L.H., 2011. Monitoring of
458 antisolvent crystallization of sodium scutellarein by combined FBRM-PVM-NIR. Journal of
459 Pharmaceutical Sciences 100, 2452-2459.

460 MacLeod, C.S., Muller, F.L., 2012. On the fracture of pharmaceutical needle-shaped crystals
461 during pressure filtration: Case studies and mechanistic understanding. Organic Process
462 Research and Development 16, 425-434.

463 O'Grady, D., O'Sullivan, B., Schoell, J., Redman, T., Barrett, M., 2008. Rapid crystallization
464 development and scale-up using in-process tools. Chimica Oggi-Chemistry Today 26, 22-24.

465 Parris, J., Airau, C., Escott, R., Rydzak, J., Crocombe, R., 2005. Monitoring API drying
466 operations with NIR. Spectroscopy 20, 34-41.

467 Peinado, A., Hammond, J., Scott, A., 2011. Development, validation and transfer of a near
468 infrared method to determine in-line the end point of a fluidised drying process for
469 commercial production batches of an approved oral solid dose pharmaceutical product.
470 Journal of Pharmaceutical and Biomedical Analysis 54, 13-20.

471 Roberts, R.J., Rowe, R.C., York, P., 1995. The relationship between the fracture properties,
472 tensile-strength and critical stress intensity factor of organic-solids and their molecular-
473 structure. International Journal of Pharmaceutics 125, 157-162.

474 Sekulic, S.S., Wakeman, J., Doherty, P., Hailey, P.A., 1998. Automated system for the on-
475 line monitoring of powder blending processes using near-infrared spectroscopy - part II.
476 Qualitative approaches to blend evaluation. Journal of Pharmaceutical and Biomedical
477 Analysis 17, 1285-1309.

478 Subero, J., Ghadiri, M., 2001. Breakage patterns of agglomerates. Powder Technology 120,
479 232-243.

480 Tewari, J., Dixit, V., Malik, K., 2010. On-line monitoring of residual solvent during the
481 pharmaceutical drying process using non-contact infrared sensor: A process analytical
482 technology (PAT) approach. Sensors and Actuators, B 144, 104-111.

483 Tok, A., Goh, X.P., Ng, W., Tan, R., 2008. Monitoring granulation rate processes using three
484 PAT tools in a pilot-scale fluidized bed. AAPS PharmSciTech 9, 1083-1091.

485 Walker, G.M., Bell, S.E.J., Greene, K., Jones, D.S., Andrews, G.P., 2009. Characterisation of
486 fluidised bed granulation processes using in-situ Raman spectroscopy. Chemical Engineering
487 Science 64, 91-98.

488 Zhang, Z., Ghadiri, M., 2002. Impact attrition of particulate solids. Part 2: Experimental
489 work. Chemical Engineering Science 57, 3671-3686.

490

491

492 **Tables**

493 Table 1. Isolation conditions for each of the experiments carried out and % LOD after each
494 phase.

495

Experiment	Pressure filtration period/ h	LOD after filtration period/ % w/w	Agitation type[a]	Agitation period/ h	LOD after agitation period/ % w/w
1	0[b]	104[b]	CA	2.167	0.05
2	0.167	22	CA	1.216	0.05
3	0.333	7	CA	1.750	0.18
4	0.500	4	CA	0.900	0.09
5	1.000	3	CA	0.500	0.35
6	0.167	40	IA	0.100	0.29
7	0.500	15	IA	0.067	0.50

496

497 [a] CA = continuous agitation and IA = intermittent agitation (1 min agitation per 0.5 h of
498 drying).
499 [b] cake left to filter for 1 h at atmospheric pressure to allow enough methanol to be removed
500 by gravity in order to start drying; LOD quoted is after 1 h period.

501

502 Table 2. Median Feret Max values obtained at the end of each drying phase for experiments 1
503 – 7.

Experiment	Agitation type[a]	QICPIC Feret Max D50 after pressure filtration[b]/ μm	QICPIC Feret Max D50 after vacuum agitated drying/ μm
1	CA	392	236
2	CA	381	216
3	CA	411	181
4	CA	391	189
5	CA	421	221
6	IA	405	343
7	IA	394	368

504

505 [a] Continuous agitation (CA) or intermittent agitation (IA) carried out during vacuum agitated
506 drying period.
507 [b] Average Feret Max D50 value for COA particles before slurries were prepared was 413 ±
508 18 μm (average ± one standard deviation based on duplicate measurements of 3 sub samples;
509 n=6).

510

511 **Figures**

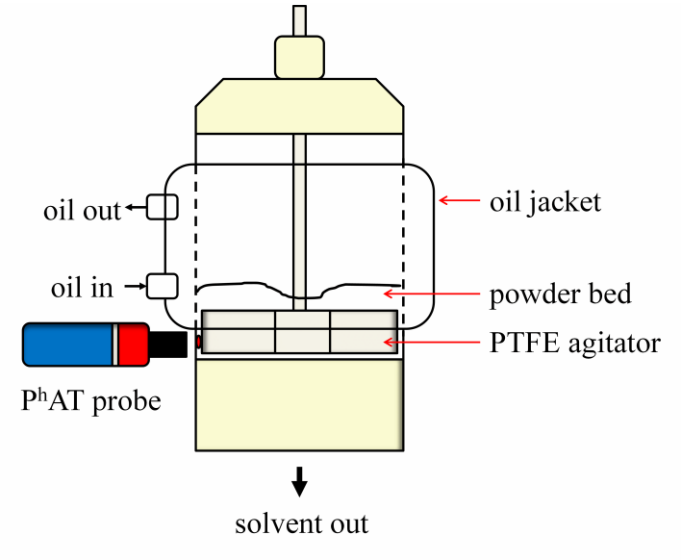

512

513 Fig.1. Schematic of the vacuum agitated filter drier. Non-invasive Raman measurements were

514 made through the glass wall beneath the oil jacket at the side of the vessel.

515

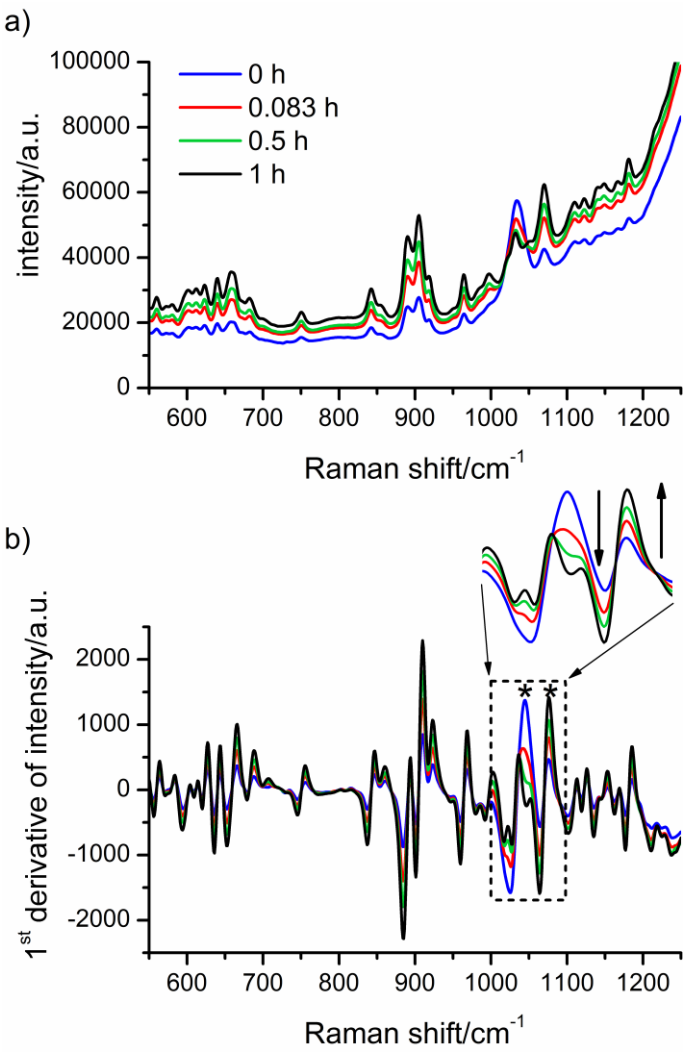

516

517 Fig. 2. Example a) underivatised and b) 1st derivative Raman spectra (550 – 1250 cm^{-1}) at
518 stated time points during 1 h pressure filtration (experiment 5): blue 0 h; red 0.083 h; green
519 0.5 h; black 1 h. * in b) indicates the peaks at 1044 and 1076 cm^{-1} which were used to
520 generate drying curves based on methanol and COA, respectively.

521

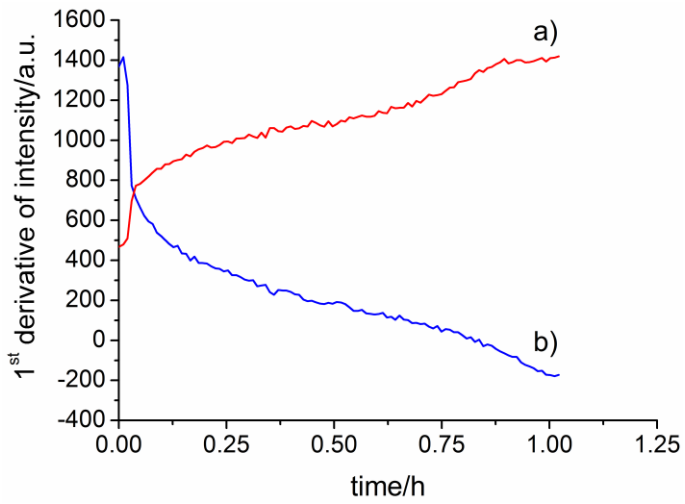

522

523 Fig. 3. Univariate drying curves from a) the COA peak centred at 1076 cm^{-1} (red) and b) the
524 methanol peak centred at 1044 cm^{-1} (blue) in the 1st derivative Raman spectra during 1 h
525 pressure filtration (experiment 5).

526

527 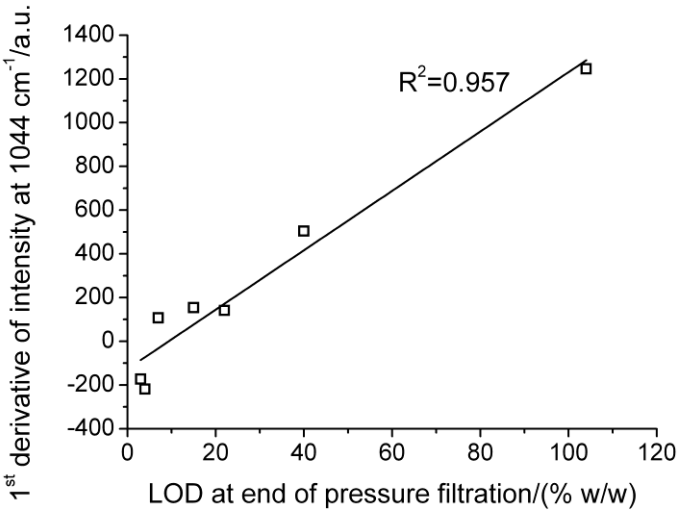

528 Fig. 4. LOD data versus the 1st derivative Raman signal of methanol at 1044 cm^{-1} at the end

529 of the N_2 pressure filtration period.

530

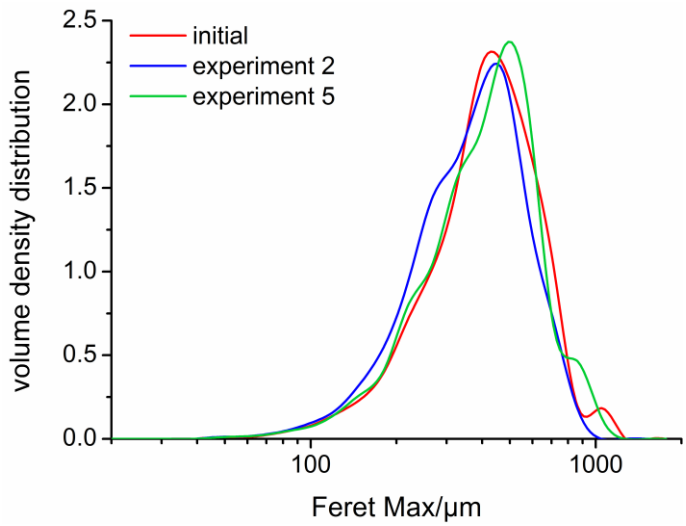

Fig. 5. Example Feret Max particle size distributions of COA for the initial particles before the slurries were prepared (red), and after pressure filtration periods of 0.167 h in experiment 2 (blue) and 1 h in experiment 5 (green).

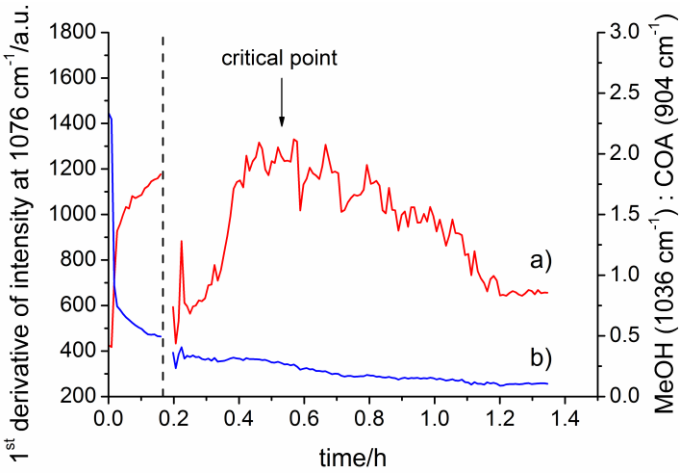

536

537 Fig. 6. Drying curves from a) 1st derivative Raman signal at 1076 cm^{-1} arising from COA
538 particles (red) and b) the ratio of methanol: COA peaks in the underivatised Raman spectra
539 (blue) from experiment 2 (continuous agitation). Dashed black line indicates the end of the
540 N_2 pressure filtration period. The discontinuity in the data occurs during the changeover
541 period from pressure filtration to vacuum drying.

542

543 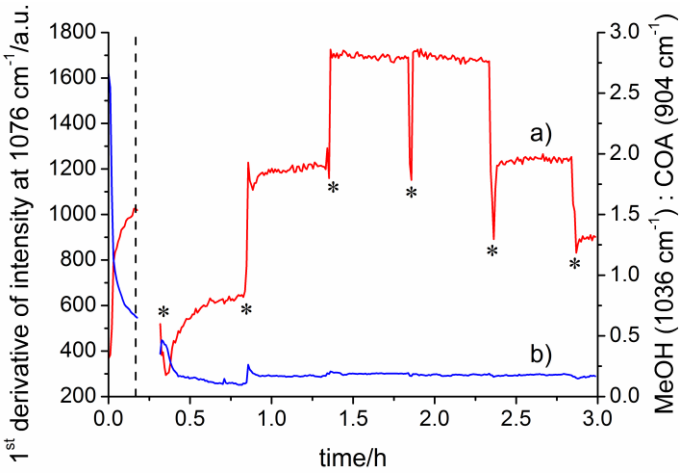

544 Fig. 7. Drying curves from a) 1st derivative Raman signal at 1076 cm^{-1} arising from COA
545 particles (red) and b) the ratio of methanol: COA peaks in the underivatised Raman spectra
546 (blue) from experiment 6 (intermittent agitation; ∗ denotes 1 min agitation periods). Dashed
547 black line indicates the end of the N_2 pressure filtration period. The discontinuity in the data
548 occurs during the changeover period from pressure filtration to vacuum drying.

549

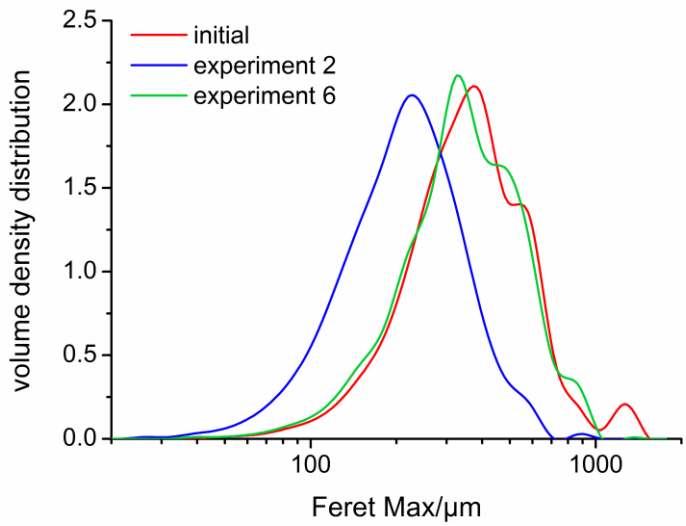

550

551 Fig. 8. Example Feret Max particle size distributions for COA before the slurries were
552 prepared (red), and after the vacuum agitated drying periods for experiments 2 (blue) and 6
553 (green).

554

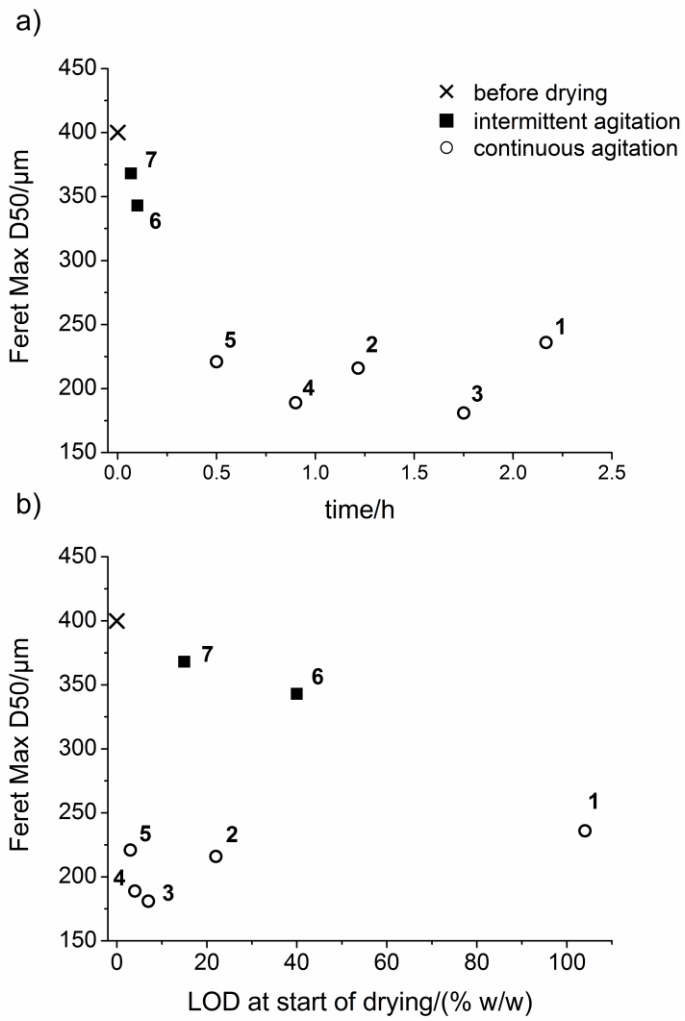

Fig. 9. QICPIC Feret Max D50 values for particles before drying (which is the average value obtained from repeat measurements of 3 sub samples of the COA batch used for the study) and after drying for experiments 1 to 7 versus a) total agitation time and b) LOD at the start of the vacuum agitated drying period (after pressure filtration).